Available online at www.sciencedirect.com
ScienceDirect
Catalysis Today 117 (2006) 329–336
CATALYSIS TODAY
www.elsevier.com/locate/cattod

In situ structural changes during toluene complete oxidation on supported $EuCoO_3$ monitored with ^{151}Eu Mössbauer spectroscopy

M. Alifanti [a], M. Florea [a], G. Filotti [b], V. Kuncser [b], V. Cortes-Corberan [c], V.I. Parvulescu [a,*]

[a] *University of Bucharest, Faculty of Chemistry, Department of Chemical Technology and Catalysis, 4-12 Regina Elisabeta Bvd., Bucharest 030016, Romania*
[b] *National Institute of Materials Physics, PO Box MG-07, 077125 Bucharest-Magurele, Romania*
[c] *Instituto de Catálisis y Petroleoquímica (CSIC), Cantoblanco, 28049 Madrid, Spain*

Available online 30 June 2006

Abstract

Ceria–zirconia supported (10 and 20 wt.% $EuCoO_3$) versus bulk $EuCoO_3$ perovskite were prepared via citrate decomposition at 700 °C and tested for toluene complete oxidation. S_{BET}, XRD, XPS, H_2-TPD and *in situ* ^{151}Eu Mössbauer investigations were performed. Electron delocalization processes around the Eu cations are induced by the reaction, as proved via the evolution of the Mössbauer parameters. All characterization data indicate the formation of a well-dispersed $EuCoO_3$ at the surface of $Ce_{0.9}Zr_{0.1}O_2$ for the 10 wt.% loading and larger crystallite formation for 20 wt.% loading. In terms of intrinsic activity for toluene combustion, supported catalysts were more active than bulk $EuCoO_3$. All structural changes during operation time are reversible.

Keywords: Supported perovskite; Ceria support; ^{151}Eu Mössbauer spectroscopy; Toluene combustion

1. Introduction

Catalytic total oxidation of various volatile organic compounds (VOC) became an interesting and stringent solution for environment protection [1]. For such purposes noble metals are mainly used but they lack thermal stability, they can be easily poisoned/deactivated and are extremely expensive [2,3]. On the other hand, mixed oxides are a suitable alternative in view of thermal stability, lower price and tunable by composition catalytic activity. Perovskite structure – ABO_3 (A—usually lanthanide, dodecahedral coordinated, B—transitional metal for catalytic purposes, octahedral coordinated) – may accommodate almost all the elements of the Periodic Table. This compositional flexibility induces interesting and useful properties and the capabilities of such materials were thoroughly studied from electrical, magnetic, optical and chemical point of view [4–10]. But only a few base-formulations are known for their activity in total oxidation reactions, namely those based on Fe, Co, Ni and Mn at B-site with La (partially substituted by other lanthanide or alkaline-earth metals) at A-site.

However, the major drawback of perovskite large-scale use for catalytic purposes is the low surface area and increased tendency to sinter at high temperatures. Deposition or embedding on adequate refractory supports is a suitable route for solving these problems [3,11–14]. The most common mesoporous supports such as alumina and silica were intensively studied. Even if stabilized with inert elements toward perovskite, components still yield catalytically inactive compounds such as spinels. Ceria-based materials and zirconia were reported as good carriers, leading to no interaction with the most common cations of perovskites [15–17]. In many occasions, they were found to provide an adequate surface area such as the case of cerium-based materials having good oxygen storage-and-release properties [18,19]. At the same time, some studies on Co-based perovskites showed that in a reductive atmosphere Co can be reduced to Co^0. This is an interesting way of preparing highly dispersed Co on lanthanide oxide active for synthesis gas production [20,21]. However, under an oxidant atmosphere, the perovskite structure is reformed [21,22].

* Corresponding author.
E-mail address: v_parvulescu@chem.unibuc.ro (V.I. Parvulescu).

0920-5861/$ – see front matter © 2006 Elsevier B.V. All rights reserved.
doi:10.1016/j.cattod.2006.05.036

The aim of this paper was to investigate the behavior of a Eu–Co-perovskite in total oxidation of toluene in *in situ* conditions. The literature is scarce reporting such studies for perovskites. Because they are black materials, it is hard to follow their behavior by using spectral techniques. In addition, the changes in the intrinsic properties of these materials are rather small when exposed to temperature, and consequently require highly sensitive techniques. One technique suitable for such a study is Mössbauer spectroscopy but it lacks the applicability for most of the interesting cations. Fortunately, ^{151}Eu is a Mössbauer atom. The idea of Eu replacement for La in Co-based perovskites is not new but the literature reported only a partial replacement. These studies indicated a beneficial effect for methane combustion [23,24]. The presence of europium in the perovskite formulation decreases the Goldschmidt tolerance factor ($t = (r_A + r_O)/[2^{1/2}(r_B + r_O)]$, considering the oxide described by formula ABO_3) and increases the reducibility of B-site cation [5,21]. Other reports dealt with fundamental studies or with comparative photocatalytic behavior of different lanthanide cations at A-site [25,26] but not with application of Eu-cobaltites for VOC total oxidation. $EuFeO_3$ was one of the most active catalysts for photocatalytic destruction of different organic dyes [26].

2. Experimental

2.1. Catalyst preparation

$Ce_{0.9}Zr_{0.1}O_2$ support and bulk $EuCoO_3$ were prepared by citrate method [27–31] from the corresponding nitrates and calcined at 700 °C for 6 h. Ten and 20 wt.% $EuCoO_3$ were deposited by incipient wetness [30]. Briefly, $Eu(NO_3)_3{\cdot}6H_2O$, $Co(NO_3)_2{\cdot}6H_2O$, and citric acid monohydrate were used as starting materials. An aqueous solution containing Eu:Co = 1:1 molar was mixed with citric acid added in 10 wt.% excess to the stoichiometric amount necessary to complexate the cations.

After a slow evaporation of water at room temperature for 24 h, the drying process was completed by heating the powder in a vacuum oven at 60 °C and 200 kPa pressure and followed by calcination at 700 °C.

2.2. Catalyst characterization

Specific surface areas were determined by nitrogen adsorption at the temperature of liquid nitrogen on a fully computerized Micromeritics ASAP 2000 instrument, using the BET formalism. The catalyst powder was degassed for 2 h at 150 °C and 0.1 Pa before each adsorption measurement. Powder XRD patterns were collected with a Kristalloflex Siemens D5000 diffractometer operating with Cu Kα radiation (λ = 1.5418 Å). Acquisition was realized in the 2θ range 2–65° with a scan step of 0.03°. XPS spectra were recorded at room temperature at a maximum pressure of 10^{-7} Pa using SSX-100 Model 206 Surface Science Instrument spectrometer with monochromatized Al Kα radiation ($h\nu$ = 1486.6 eV). Charge correction was made considering the C 1s signal of contaminating carbon (C–C or C–H bonds) at 284.8 eV. Local electronic phenomena and electron delocalization processes around the Eu ions induced by calcination were studied by ^{151}Eu Mössbauer spectroscopy at 22 °C. The catalysts activation and the influence of the surrounding environment at 350 °C were *in situ* monitorized using this technique, both in air and reaction mixture (air + toluene) atmosphere. The *in situ* experiments were carried out by inserting the catalysts in an oven with Be windows transparent to the γ radiation. A Mössbauer drive system operating in constant acceleration mode combined with conventional electronics and a $^{151}Sm_2O_3$ source with an activity of about 85 mCi was employed. The typical γ radiation of 21.6 keV (emitted by the relaxation of the excited level of ^{151}Eu on the nuclear ground level) was used. The reducibility properties of the different catalysts were studied by temperature-programmed reduction (H_2-TPR) using a ChemBET 3000 (Quanta Chrome Corporation) equipment provided with a quartz tubular reactor (i.d. = 10 mm). Samples of about 50 mg were first flushed under He flow (20 ml/min) to remove the oxygen and physically adsorbed or weakly bonded species. Subsequently, the samples were contacted with a flow of 5% H_2/Ar (20 ml/min) and heated at a rate of 10 °C/min up to 900 °C.

2.3. Catalytic activity measurement

Separate experiments concerning toluene complete oxidation were performed in a 10 mm i.d. quartz tubular reactor operating at atmospheric pressure. 0.1 g of powder catalyst was deposited between two quartz wool plugs. Prior to each catalytic activity evaluation, the catalyst was flushed with air flowing at 100 ml/min for 1 h at 600 °C, in order to remove adsorbed species and to decompose residual carbonaceous deposits at the surface, and then cooled down to 100 °C. A flow of 100 ml/min containing 1700 ppm volume of toluene in air was admitted and the temperature was raised up in steps of 25–600 °C. The CO_2 evolution in the outlet was continuously monitored by an on-line coupled Fisher–Rosemount analyzer. CO and hydrocarbons production was not evidenced by using a Porapaq Q column mounted on an HP 5890 Series II GC equipped with a TCD detector. The only reaction products were CO_2 and H_2O. Light-off curves were recorded by increasing the reaction temperature after CO_2 in the outlet reached a constant level (typically after 25–30 min). For all catalysts the descendant light-off curves superposed over the ascendant ones.

3. Results

3.1. Textural measurements

Textural investigations showed the increase of the exposed surface of $EuCoO_3$ for the contact with the reactant by perovskite deposition on $Ce_{0.9}Zr_{0.1}O_2$ (Table 1). Both supported samples showed a smaller surface area with respect to the support alone. This decrease of the surface area with the loading might indicate a preferential deposition of $EuCoO_3$ perovskite at the external surface of the support associated with some pore blocking. In order to determine the reasons of these textural changes induced by $EuCoO_3$ deposition, separate experiments using the pure support and the same amount of water as in the case of perovskite impregnation followed by the same thermal treatment were

Table 1
Textural, XPS, and activity data for bulk and supported materials

Solid	S_{BET} (m^2/g)	Eu $4d_{5/2}$ (eV)	Co $2p_{3/2}$ (eV)	XPS[Co/Eu] (at.)
$Ce_{0.9}Zr_{0.1}O_2$	37.9	–	–	–
$EuCoO_3$	14.9	135.4	780.1	0.52
10 wt.% $EuCoO_3$	28.2	135.6	779.8	0.40
20 wt.% $EuCoO_3$	24.0	135.7	780.0	0.48

performed. The surface area of "water impregnated" support was 36.7 m^2/g, indicating that textural modifications observed after $EuCoO_3$ deposition were linked exclusively to the presence of $EuCoO_3$. Indeed, the surface area of bulk $EuCoO_3$ is less than half of the surface area of the support and the results from Table 1 very likely indicate the fact that the impregnated phase is located at the external surface of the support grains, blocking a part of the carrier oxide pores.

3.2. XRD investigation

All synthesized materials were crystalline after calcination at 700 °C. Bulk $EuCoO_3$ crystallized in a perovskite orthorhombic symmetry (JCPD 25-1054) (Fig. 1a). XRD analysis performed on 20 wt.% $EuCoO_3/Ce_{0.9}Zr_{0.1}O_2$ showed the strong signals of the support (Fig. 1b). $EuCoO_3$ formation could be followed by means of the very weak lines assigned to perovskite phase (Fig. 1b) centered at 23.9°, 42.26°, 50.2° and to the asymmetry of the (2 2 0) reflection plane of $Ce_{0.9}Zr_{0.1}O_2$ support at 33.15°, due to the overlapping of the main reflection plane of $EuCoO_3$ plane centered at 33.92°. On 10 wt.% $EuCoO_3$ sample no perovskite diffraction lines could be observed (pattern not shown). Based on the above considerations and to previous results obtained on $LaCoO_3/Ce_{0.8}Zr_{0.2}O_2$ system [17] where perovskite phase signals could be observed for loadings higher than 15 wt.%, a high dispersion associated to small crystallite size of the deposited phase might be supposed for the low perovskite loading.

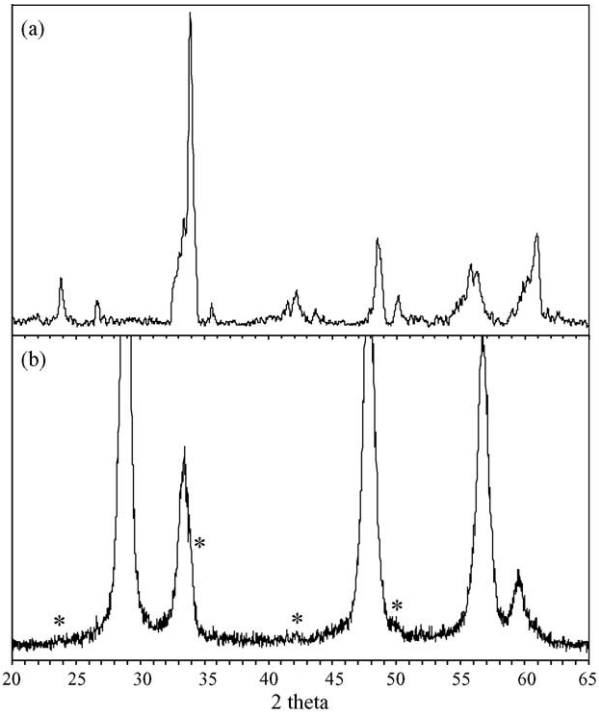

Fig. 1. XRD pattern for bulk $EuCoO_3$ (a) and 20 wt.% $EuCoO_3/Ce_{0.9}Zr_{0.1}O_2$ (b); (*) $EuCoO_3$ perovskite phase.

3.3. XPS results

Table 1 also compiles data obtained by XPS. The binding energies are in the ranges characteristic to 3+ oxidation state for both Eu and Co. In the case of supported $EuCoO_3$ the position of Eu and Co signals, identical to those observed from Eu and Co in the bulk $EuCoO_3$, suggest no specific interaction of with Ce or Zr the support. This, together with XRD patterns, may suggest the formation of a clean perovskite phase, as previously observed for supported $LaCoO_3$ using the corresponding citrates as precursors [17,30]. A confirmation of the perovskite phase formation at the surface of the $Ce_{0.9}Zr_{0.1}O_2$ is brought by the [Co/Eu] atomic ratio which is close to the value observed for bulk $EuCoO_3$ (Table 1). However, the larger deviation observed for 10 wt.% loading (0.40 with respect to 0.52) might be linked to the low quality of the signals of Eu and Co due to a deeper penetration into the pores as could be supposed based on the surface area values which made the quantitative atomic surface composition subject of errors [17].

3.4. H_2-TPD

Fig. 2 shows the dynamic H_2-TPR profiles recorded both for bulk and the two supported $EuCoO_3$ samples. A clear difference in the reduction profiles can be observed comparing bulk material with the supported ones.

The H_2O production during TPR experiment on bulk $EuCoO_3$ was bimodal, with two main peaks centered at 400 and 570 °C (Fig. 2a). The high-temperature peak is asymmetric, with the maximum at 563 °C and a drop leveling off at 625 °C. Fig. 2b shows the hydrogen uptake curve that follows a similar bimodal pattern. The two peaks of hydrogen uptake evolved at the same temperatures as the water formation signals. This behavior pointed to no strong phenomenon of formed water adsorption or re-adsorption. On hydrogen consumption curve it can be also seen a clear double contribution in the high-temperature peak, the second maximum in Fig. 2b superposing on the shoulder at 625 °C in Fig. 2a. This might indicate the occurrence of mass transport phenomena, either for H_2 penetration to the bulk or H_2O elimination from the lattice.

The catalytic literature scarcely report TPR studies the Eu-based materials [32]. It is feasible to consider that $EuCoO_3$ follows a similar reduction pattern with $LaCoO_3$ since europium oxide is a hard reducible oxide as lanthania [21]. Consequently, the TPR signals were assigned to Co^{3+} progressive reduction. The two peaks were attributed to $Co^{3+} \rightarrow Co^{2+}$ reduction in a first step, followed by the reduction to Co^0 at a higher temperatures. The results are consistent to those obtained by Huang et al. [33] and Lago et al. [21]. As in those cases the relative area of the peak at 400 °C is approximately half of that evolved at the highest

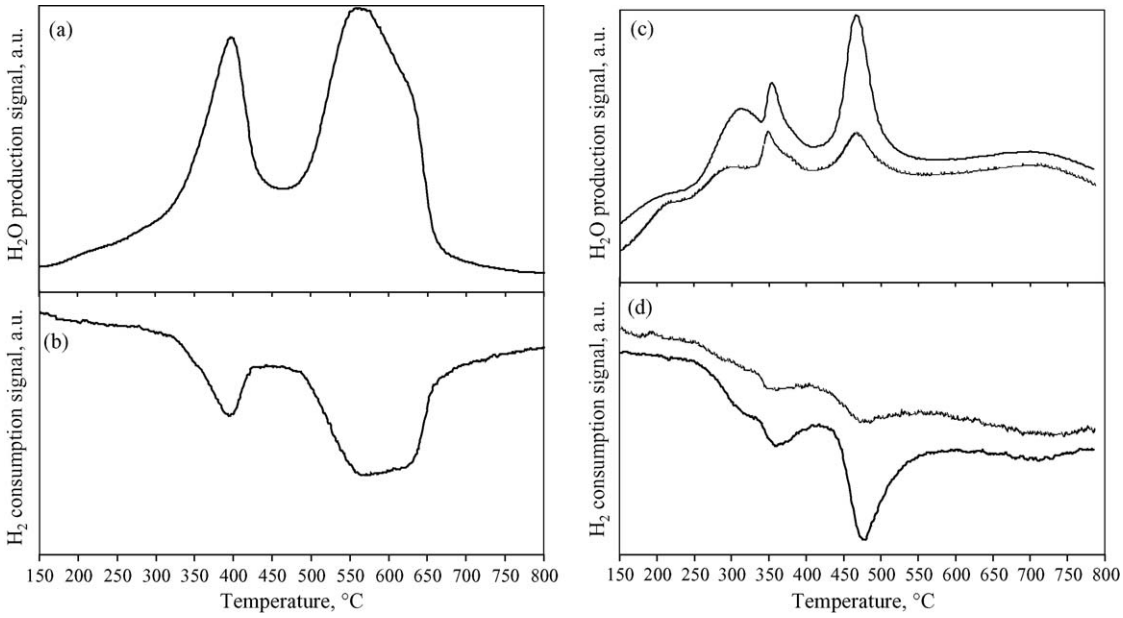

Fig. 2. H_2-TPD profiles for bulk (a and b) and supported (c and d) $EuCoO_3$; (a and c) H_2O ($m/z = 18$) evolution profile, (b and d) H_2 ($m/z = 2$) evolution profile; (c and d) thin line 10 wt.% $EuCoO_3/Ce_{0.9}Zr_{0.1}O_2$, heavy line 20 wt.% $EuCoO_3/Ce_{0.9}Zr_{0.1}O_2$.

temperatures and by correlation with XPS may support a stepwise reduction of Co.

From the study of Lago et al. [21] was observed a trend with the decreasing of the cationic radius of the lanthanide: the smaller the radius the smaller was the reduction temperature characteristic to the higher temperature peak. The first reduction step occurred at the same temperature (around 360 °C in their case) irrespective to the lanthanide nature. Since Eu is placed between Sm and Gd it may be assumed that the maximum for $EuCoO_3$ would be placed between the two values obtained for $SmCoO_3$ (512 °C) and $GdCoO_3$ (500 °C). Applying a correction of 40 °C (considering the first reduction peak evolved at 360 °C in [21]) it will result a very good concordance with literature data for the $Co^{2+} \rightarrow Co^0$ reduction. Also, the departure between the two peaks is in the range reported previously for lanthanide cobaltites, namely, around 170 °C [21,33]. We underline that the compared catalysts exhibited surface areas around 10 m^2/g.

H_2-TPR profiles of supported samples are reprised in Fig. 2c and d. The maxima are superposed over the two main peaks of H_2O evolution, pointing to no strong adsorption or re-adsorption of water on these composite materials. H_2-TPR profiles changed with the increase of the $EuCoO_3$ loading, modifications in the intensity being observed for the peaks centered around 310 and 467 °C. It seems feasible to assign these two peaks to the two-step reduction of the perovskite phase, as for the aforementioned bulk $EuCoO_3$. The different amount of evolved water (or H_2 uptake) and the sharpening of the peaks as the perovskite loading increased indicate an effect of the dispersion, i.e. of the perovskite particle size, on the Co reducibility. It was already suggested that broad reduction peaks account for the existence of a bimodal particle size distribution [34]. The broad peaks for 10 wt.% $EuCoO_3/Ce_{0.9}Zr_{0.1}O_2$ may also account for the occurrence of some diffusional effects, very likely from the water migration from pores. For loadings of 20 wt.% the amount of perovskite at the external surface is significantly higher and the peaks come mainly from the reduction of the perovskite larger crystallites [17] located outside the pores.

The peak at 350 °C, almost similar for the both supported catalysts, is generated by the superficial reduction of ceria support, while the large peak at around 700 °C corresponds to the reduction of bulk Ce^{4+} [35,36].

3.5. *In situ* Mössbauer

Apart dynamic H_2-TPR, *in situ* Mössbauer experiments under reaction conditions were done in order to have a deeper insight on the whole perovskite components behavior, more specifically looking for Eu.

Table 2 compiles some representative Mössbauer parameters collected at 22 °C in air on the precursors and the supported perovskites, as resulted after fitting spectra with a NORMOS package, using the full perturbation Hamiltonian [37]. The quadrupole splitting (QS) gives information about the charge symmetry (either electronic or ionic) around the central Eu cation whereas the linewidth of the absorption line is dependent

Table 2
The Mössbauer parameters of the spectra shown in Fig. 3 (left) (*w*—absorption linewidth)

Sample	QS (mm/s)	IS (mm/s)	*w* (mm/s)
20 wt.% $EuCoO_3$-precursor	2.8 (1)	−0.60 (7)	2.0 (1)
20 wt.% $EuCoO_3$	2.5 (1)	0.00 (5)	2.4 (1)
10 wt.% $EuCoO_3$-precursor	1.3 (1)	−0.40 (5)	2.3 (1)
10 wt.% $EuCoO_3$	3.0 (1)	0.01 (5)	2.1 (1)

Absolute errors (given in brackets) are about 0.1 mm/s for QS and *w*, and less than 0.1 mm/s for IS.

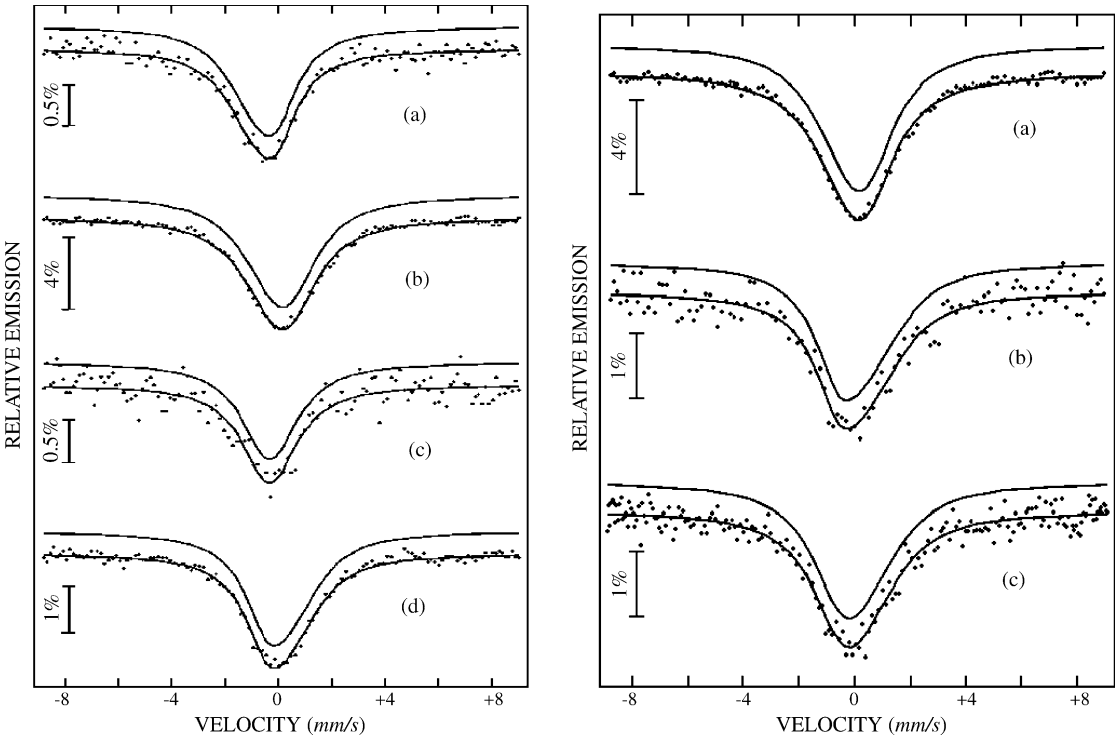

Fig. 3. ^{151}Eu Mössbauer spectra for: 10 wt.% $EuCoO_3/Ce_{0.9}Zr_{0.1}O_2$ (a) non-calcined, (b) calcined; 20 wt.% $EuCoO_3/Ce_{0.9}Zr_{0.1}O_2$ (c) non-calcined, (d) calcined, all at 22 °C (left), and for 20 wt.% $EuCoO_3/Ce_{0.9}Zr_{0.1}O_2$ in different atmospheres: (a) 22 °C, air; (b) 350 °C, air; (c) 350 °C, toluene (right).

on both the lifetime of the nucleus on the excited state as well as on the defect distribution around the Eu cation. Finally, the most important Mössbauer parameter in our discussion is the isomer shift, IS. There are two contributions to the isomer shift: (i) one due to the electronic configuration, called the chemical isomer shift and (ii) another due to the vibration state of the Eu atoms in the solid, called the thermal shift or alternatively, the second order Doppler shift (SOD). The last contribution is temperature dependent and a correction of the experimental IS through SOD is required, in order to compare the various chemical configurations at different temperatures. IS is very sensitive to the oxidation state of the Eu ions. For Eu^{2+} ions it is about −12 mm/s whereas for an Eu^{2+} is about 0 mm/s. As IS can be obtained with a precision exceeding 0.1 mm/s, the ^{151}Eu Mössbauer spectroscopy becomes a very sensitive tool for studying electron delocalization processes or charge transfer phenomena around the Eu site.

Typical IS for Eu^{3+} ions are presented in Table 2. Higher values (closer to zero) were obtained for the supported calcined samples, as an indication of a higher oxidation process of Eu ions induced via calcination. The degree of oxidation is increased in the calcined sample with the perovskite content (IS increases from −0.6 to 0.0 in sample with 20 wt.% $EuCoO_3$ as compared with an increase from −0.4 to 0.0 in sample with 10 wt.% $EuCoO_3$).

The ^{151}Eu Mössbauer spectra of 20 wt.% $EuCoO_3$ sample collected at 22 and 350 °C in air and in reaction mixture are shown in Fig. 3 (right). It is worth to mention that the reaction was developed over 72 h, which corresponds also to the acquisition time. The hyperfine parameters resulted from the fitting of the Mössbauer spectra shown in Fig. 3 (right) are presented in Table 3. Slightly higher quadrupole splitting and linewidths are induced at 350 °C due to the distortion of the lattice. At a first view, no significant variation can be mentioned for the experimentally obtained isomer shifts (0.00(5) mm/s at 22 °C and 0.01(5) and −0.15(5) mm/s at 350 °C, in different atmospheres). At this point it is worth to mention that in order to compare the chemical configurations in the two situations (in the absence and the presence of the reaction), the IS obtained at 22 °C (no activated reaction) should be extrapolated at 350 °C within the assumption of no chemical changes: that is, only the SOD correction has to be applied.

Table 3
The Mössbauer parameters deduced from the 20 wt.% $EuCoO_3/Ce_{0.9}Zr_{0.1}O_2$ spectra shown in Fig. 3 (right) (*w*—absorption line width)

Experimental conditions	QS (mm/s)	IS (mm/s)	*w* (mm/s)
22 °C (extrapolation at 350 °C (SOD considered))	2.5 (1)	−0.00 (5), −0.30 (5)	2.0 (1)
350 °C, air	3.8 (1)	0.01 (5)	2.4 (1)
350 °C, air + toluene	2.9 (1)	−0.15 (5)	2.3 (1)

Absolute errors (given in brackets) are about 0.1 mm/s for QS and *w*, and less than 0.1 mm/s for IS.

In average, a decrease of the isomer shift due to the second order Doppler shift with about 0.30 mm/s over an increase in temperature of about 330 °C could be considered [38–40]. Therefore, by default, an isomer shift of −0.30(5) mm/s is assumed for 20 wt.% $EuCoO_3$ at 350 °C. This value has to be compared with 0.01(5) mm/s for the Eu electronic configuration during thermal treatment in air and, respectively, with −0.15(5) mm/s for the Eu electron configuration in the reaction mixture. Obviously, heating induces an oxidation process at the Eu site (delocalization of 4f electrons from the Eu^{3+} ions) and this process is enhanced by the air atmosphere (IS increases from −0.30(5) to 0.01(5) mm/s) as compared to the results obtained in reaction mixture (IS increases from −0.30(5) to only −0.15(5) mm/s).

Several cycles of measurement of ^{151}Eu Mössbauer signal in air and reaction mixture showed a reversibility of the atoms distribution around Eu ions, the signals being similar to those in Fig. 3b (right).

3.6. Catalytic activity

Table 4 compares the catalytic activity of $EuCoO_3$, in bulk and supported form for the total oxidation of toluene. All catalysts, including the support alone, completely convert toluene at temperatures below 500 °C. If the activity is expressed by T_{50} (deduced by the light-off curves) the most active catalyst is 20 wt.% $EuCoO_3$, that lowers the light-off temperature with 20 °C with respect to bulk $EuCoO_3$. The trend is similar to that observed for supported $LaCoO_3$ [30]. Interestingly, the 10 wt.% $EuCoO_3/Ce_{0.9}Zr_{0.1}O_2$ presents a T_{50} higher with only 12 °C with respect to bulk perovskite while in the case of 10 wt.% $LaCoO_3/Ce_{0.9}Zr_{0.1}O_2$ the temperature was 40 °C higher. But, the diminishing of the T_{50} for 20 wt.% loading of perovskite was with only 20 °C for $EuCoO_3$ with respect to $LaCoO_3$ (40 °C), under similar conditions [30]. However, this effect occurred at a less intensity for 20 wt.% $EuCoO_3$ catalyst.

A deeper insight in the effects induced by the perovskite deposition can be obtained considering the reaction rates expressed per mass unit of perovskite. The specific reaction rates were calculated from the corresponding Arrhenius plots. Due to the large excess of oxygen, a first order kinetics with respect to toluene and zero order with respect to oxygen were applied for a plug-flow reactor [30]. The experimental conversions in the 10–90% range were considered and all Arrhenius plots were linear. The results derived for a temperature of 300 °C are reprised in Table 4. For a better comparison, the reaction rates on pure support and on bulk $EuCoO_3$ are also showed. The increase of the $EuCoO_3$ activity is spectacular by deposition on the support, namely, with a factor of 8 and 12 for 10 and 20 wt.% loading, respectively (Table 4). The descendant light-off curves superposed over the light-off curves recorded for increasing temperature pointing to a stable structure of $EuCoO_3/Ce_{0.9}Zr_{0.1}O_2$ materials.

Table 4
Activity data for bulk and supported materials

Solid	T_{50}	Reaction rate at 300 °C (μmol s^{-1} $g^{-1}_{perovskite}$)
$Ce_{0.9}Zr_{0.1}O_2$	295	0.82
$EuCoO_3$ ($LaCoO_3$)	256 (2 4 4)	1.2 (1.6)
10 wt.% $EuCoO_3$ ($LaCoO_3$)	268 (2 8 4)	9.4 (13.3)
20 wt.% $EuCoO_3$ ($LaCoO_3$)	234 (2 0 0)	15.2 (20.5)

Values in the brackets are taken from [30].

4. Discussions

XRD patterns of $EuCoO_3$ in both bulk and supported form account for an orthorhombic symmetry. No structural changes occurred by deposition on the $Ce_{0.9}Zr_{0.1}O_2$ support accounting for a non-specific interaction between the perovskite components and ceria. Previous results for $LaCoO_3$ and $LaMnO_3$ materials showed a rhombohedral symmetry of the lattice that was preserved after deposition on ceria-based supports [27,41]. The change of symmetry for Co-based perovskites is not unexpected since the ionic radius of Eu^{3+} is significantly smaller than that of La^{3+} (0.95 and 1.06 Å, respectively) leading to a decrease of the volume cell [42,43]. This change in the ionic radii led to a change in the value of the tolerance factor t ($t = (r_A + r_O)/[2^{1/2}(r_B + r_O)]$) and consequently to a change in the lattice symmetry. Considering only geometric factors, $LaCoO_3$ is the most stable Co-based perovskite while in $EuCoO_3$ the reducibility of Co increased mainly due to the lattice symmetry change [21], as proven by the TPR profile.

After the deposition onto the ceria–zirconia support via impregnation with an $EuCoO_3$ sol, XRD patterns evidenced the presence of the perovskite only for loadings higher than 20 wt.%. Corroborated with the broadening of the reflections of the supported perovskite and the absence of the reflection lines of any individual Eu or Co oxide, this may suggest that in the supported structures the perovskite exists mostly as nanoparticles. XPS gave additional arguments in this sense showing that the binding energies and Eu/Co ratios are similar with those in pure perovskite. Also, XPS indicated that the $EuCoO_3$ perovskite phase is not uniformly spread at the support surface, which is in agreement with previous results [30].

TPR profiles of both supported samples correspond to a pattern that is different and more complex than that of bulk $EuCoO_3$ (Fig. 2). The peaks corresponding to $EuCoO_3$ reduction are shifted to smaller temperatures, and for that located at smaller temperatures a contribution of the support reduction is partially overlapped. This behavior demonstrated an effect of dispersion upon reducibility as previously reported for Co_3O_4 [44].

Total oxidation of hydrocarbons on transitional metal oxides is a reaction supposed to obey a Mars-van Krevelen mechanism [45,46]. Therefore, the capacity to release oxygen offers a good image on their oxidative properties. A comparative study of $LnCoO_3$ (Ln = La, Eu) oxidative behavior showed a faster decomposition of $EuCoO_3$ to Co^0 and Eu_2O_3 comparatively to $LaCoO_3$ [32]. However the $LaCoO_3$ reduction mechanism is still unclear. Several factors, like the reducing agent, heating rate or flow-rate can influence the reduction mechanism and consequently the reduction profile [44]. However, the similar

bimodal reduction profile of bulk $EuCoO_3$ may account for a similar reduction mechanism [21,33].

The catalytic experiments indicated that both bulk and supported $EuCoO_3$ were active catalysts for total oxidation of toluene. This behavior is not unexpected since Co-based perovskites were reported as very active catalysts for hydrocarbons combustion [4,5,30]. It is possible that the higher reducibility of Co, induced by the concerted action of Eu and deposition on support, is responsible for the little difference between T_{50} of bulk and 10 wt.% $EuCoO_3$, with respect to the similar $LaCoO_3$ catalysts observed in a previous work (Table 4) [30]. The higher difference observed for the 20 wt.% loading might be due mostly to a lower dispersion of $EuCoO_3$ compared to $LaCoO_3$. Assuming that toluene total oxidation obeys a Mars-van Krevelen mechanism [45,46] in which the first step is the lattice oxygen extraction, the specific activity should be correlated with the TPR results. Indeed, the comparison of these data with the reaction rate confirmed the higher activity of supported perovskites and the order: 20 wt.% $EuCoO_3$ > 10 wt.% $EuCoO_3$ (Fig. 2).

Perovskite structure is a flexible one, structural changes occurring at higher temperatures or in different environments being reversible. The descendant light-off curves superposed over the light-off curves recorded for increasing temperatures confirmed that structural changes observed in Mössbauer spectra and induced by temperature and toluene presence in the measurement environment are reversible.

Actually, the *in situ* experiments using ^{131}Eu Mössbauer spectroscopy gave answers to all the questions about the reaction mechanism and participation of A-site cation in toluene complete oxidation. $EuCoO_3$ exhibits an orthorhombic structure with *Pbnm* space group symmetry. The transition metals show octahedral oxygen coordination whereas the rare-earth atoms have 12 symmetrical oxygen neighbors. Therefore, an insignificant lattice contribution to the electric field gradient at the Eu atoms occurs in $EuCoO_3$ giving rise to a very small quadrupole splitting (high charge symmetry around the Eu cation). ^{151}Eu Mössbauer spectra consisting in only one shaped and large central absorption (due to the strong superposition of the seven absorption lines raised up by the small quadrupole interactions and the lack of effective magnetic moment) were obtained both at 22 and 350 °C (Fig. 3). Mössbauer parameters of Eu spectra recorded at 350 °C in air, pointed to a dislocation of 4f electrons of Eu^{3+} associated with a slow ''oxidation'' (the chemical isomer shift increased by about 0.31 mm/s) while in the presence of a mixture air–toluene the chemical isomer shift increased by only 0.15 mm/s. This clearly indicates a partial relative reduction of Eu ion by the mixture air–toluene and consequently accounts for the participation of A-site cations of the perovskite structure in the total oxidation reactions. These results are especially interesting since it is generally accepted that only cations on the B-position are responsible for the catalytic activity, the A-cation having just the role of tuning agent for catalytic activity. Our data bring experimental evidences that the electronic configuration of the A-site cation is changed during reaction, accounting for its chemical participation in a more active way than presumed.

Some measurement cycles in the presence and in the absence of toluene in the feed mixture showed a ^{151}Eu Mössbauer signal not affected by the total oxidation reaction. The removal of toluene from the gas flow led to a local electron distribution around Eu ions similar to its initial state. A similar effect was previously observed by XRD measurements on different temperature-programmed reoxidized $LnCoO_3$ perovskite after programmed reduction. It pointed to a reversibility of the reduction effect and to the flexibility of perovskite structure [21,22].

5. Conclusions

Bulk versus supported $EuCoO_3$ perovskites were prepared by citrate method and tested for toluene complete oxidation. A pure perovskite phase is formed at 700 °C and it was evidenced by XRD and XPS investigations. Deposition via citrate precursors preserves the perovskite structure with no specific interaction with the support. The deposition of $EuCoO_3$ on ceria–zirconia support led to several advantages: the increase of the surface area by comparing with bulk perovskite and the increase of the dispersion of the active phase.

TPR experiments showed a strong effect of Eu on the oxidative properties of Co-based perovskites, decreasing the reduction temperature of Co with respect to $LaCoO_3$. Deposition of $EuCoO_3$ increases this effect, lowering the reduction temperature of Co with about 80 °C compared to bulk $EuCoO_3$. This behavior is considered to be responsible for catalytic activity improvement for supported $EuCoO_3$. Bulk and ceria supported $EuCoO_3$ perovskites are active catalysts for total oxidation of toluene. Mössbauer investigations on supported $EuCoO_3$ perovskites pointed to the occurrence of a Mars-van Krevelen oxidation mechanism for toluene complete oxidation. Also, Mössbauer data enlarged the picture of the perovskite behavior generally achieved only from TPR experiments.

References

[1] F. Garin, Catal. Today 89 (2004) 255.
[2] M.F.M. Zwinkels, S.G. Järas, P.G. Menon, T.A. Griffin, Catal. Rev. Sci. Eng. 35 (1993) 319.
[3] P.O. Thevenin, A.G. Ersson, H.M. Kusar, P.G. Menon, S.G. Jaras, Appl. Catal. A: Gen. 212 (2001) 189.
[4] J.M.D. Tascon, J.L.G. Fierro, L.J. Tejuca, in: L.J. Tejuca, J.L.G. Fierro (Eds.), Properties and Applications of Perovskite Type Oxides, Marcel Dekker, New York, 1993.
[5] M.A. Peña, J.L.G. Fierro, Chem. Rev. 101 (2001) 1981.
[6] J. Baier, S. Jodlauk, M. Kriener, A. Reichl, C. Zobel, H. Kierspel, A. Freimuth, T. Lorenz, Phys. Rev. B 71 (2005) 014443.
[7] S. Uhlenbruck, F. Tietz, Mater. Sci. Eng. B 107 (2004) 277.
[8] T. Ishihara, T. Shibayama, M. Honda, H. Nishiguchi, Y. Takita, J. Electrochem. Soc. 147 (2000) 1332.
[9] H. Falcon, A.E. Goeta, G. Punte, R.E. Carbonio, J. Solid State Chem. 133 (1997) 379.
[10] K.A. Señaris-Rodriguez, J.B. Goodenough, J. Solid State Chem. 118 (1993) 323.
[11] D. Klvana, J. Kirchnerova, J. Chaouki, J. Delval, W. Yaici, Catal. Today 47 (1999) 115.
[12] R. Schneider, D. Kiessling, G. Wendt, W. Burckhardt, G. Winterstein, Catal. Today 47 (1999) 429.

[13] P.K. Gallagher, D.W. Johnson Jr., F. Schrey, Mater. Res. Bull. 9 (1974) 1345.
[14] S.D. Peter, E. Garbowski, V. Perrichon, M. Primet, Catal. Lett. 70 (2000) 27.
[15] S. Colonna, D. De Rossi, M. Faticanti, I. Pettiti, P. Porta, J. Mol. Catal. A: Chem. 187 (2002) 269.
[16] S. Cimino, S. Colonna, S. De Rossi, M. Faticanti, L. Lisi, I. Pettiti, P. Porta, J. Catal. 205 (2002) 309.
[17] M. Alifanti, N. Blangenois, M. Florea, B. Delmon, Appl. Catal. A: Gen. 280 (2005) 255.
[18] C. Larese, M. López Granados, R. Mariscal, J.L.G. Fierro, P.S. Lambrou, A.M. Efstathiou, Appl. Catal. B: Environ. 59 (2005) 13.
[19] A. Trovarelli, C. de Leitenburg, G. Dolcetti, Chemtech (1997) 32.
[20] V.R. Choudhary, A.M. Rajput, V.H. Rane, Catal. Lett. 16 (1992) 269.
[21] R. Lago, G. Bini, M.A. Peña, J.L.G. Fierro, J. Catal. 167 (1997) 198.
[22] L. Simonot, F. Garin, G. Maire, Appl. Catal. B: Environ. 11 (1997) 167.
[23] D. Ferri, L. Forni, Appl. Catal. B: Environ. 16 (1998) 119.
[24] R. Leanza, I. Rossetti, L. Fabbrini, C. Oliva, L. Forni, Appl. Catal. B: Environ. 28 (2000) 55.
[25] A. Kudo, A. Tanaka, K. Domen, T. Onishi, J. Catal. 111 (1988) 296.
[26] X. Niu, H. Li, G. Liu, J. Mol. Catal. A: Chem. 232 (2005) 89.
[27] J. Kirchnerova, M. Alifanti, B. Delmon, Appl. Catal. A: Gen. 231 (2002) 65.
[28] H.M. Zhang, Y. Teraoka, N. Yamazoe, Chem. Lett. (1987) 665.
[29] J.W. Geus, J.C. van Giezen, Catal. Today 47 (1999) 169.
[30] M. Alifanti, M. Florea, S. Somacescu, V.I. Parvulescu, Appl. Catal. B: Environ. 60 (2005) 33.
[31] M. Alifanti, B. Baps, N. Blangenois, J. Naud, P. Grange, B. Delmon, Chem. Mater. 15 (2003) 395.
[32] Y. Wu, S. Motoi, S. Sugiyama, T. Matsuda, Y. Yoshida, Nippon Kagaku Kaishi 9 (2000) 613.
[33] L. Huang, M. Bassir, S. Kaliaguine, Appl. Surf. Sci. 243 (2005) 360.
[34] L.F. Liotta, G. Pantaleo, G. Di Carlo, G. Marcy, G. Deganello, Appl. Catal. B: Environ. 52 (2004) 1.
[35] F. Giordano, A. Trovarelli, C. de Leitenburg, M. Giona, J. Catal. 193 (2000) 273.
[36] S. Damyanova, C.A. Perez, M. Schmal, J.M.C. Bueno, Appl. Catal. A: Gen. 234 (2002) 271.
[37] R.A. Brand, Nucl. Instr. Meth. Phys. Res. B 28 (398) (1987), the NORMOS program is available from WISSEL GmbH, D-82319 Starnberg, Germany.
[38] G. Gerth, P. Kienle, K. Luchner, Phys. Lett. 27A (1968) 557.
[39] Steichele, Z. Phys. 201 (1967) 331.
[40] F.A. Deeney, J.A. Delaney, V.P. Ruddy, Phys. Lett. 27A (1968) 571.
[41] M. Alifanti, J. Kirchnerova, B. Delmon, Appl. Catal. A: Gen. 245 (2003) 231.
[42] J. Baier, S. Jodlauk, M. Kriener, A. Reichl, C. Zobel, H. Kierspel, A. Freimuth, T. Lorenz, Phys. Rev. B 71 (2005) 014443.
[43] S. Uhlenbruck, F. Tietz, Mater. Sci. Eng. B 107 (2004) 277.
[44] G. Jacobs, T.K. Das, Y.Q. Zhang, J.L. Li, G. Racoillet, B.H. Davis, Appl. Catal. A: Gen. 233 (2002) 263.
[45] M. Alifanti, J. Kirchnerova, B. Delmon, D. Klvana, Appl. Catal. A: Gen. 262 (2004) 167.
[46] N. Bahlawane, E. Fischer-Rivera, K. Kohse-Höinghaus, A. Brechling, U. Klein, Appl. Catal. B: Environ. 53 (2004) 245.